RSC Advances

PAPER

Manganese dioxide nanowires on carbon nanofiber frameworks for efficient electrochemical device electrodes†

Y. Saito,[a] M. Meguro,[a] M. Ashizawa,[a] K. Waki,[b] R. Yuksel,[c] H. E. Unalan[d] and H. Matsumoto*[a]

Hierarchically nanostructured composite electrodes were prepared by the electrodeposition of manganese dioxide nanowires (MnO_2 NWs) with 5–20 nm diameters on electrospun carbon nanofiber (CNF) webs with diameters of 250 and 650 nm. The effects of CNF diameters and mass loading of MnO_2 NWs on the hierarchical nanostructure formation and the performance of the composite electrodes were investigated. The internal structure of the composite electrode depended on CNF diameter and mass loading of MnO_2 NW. The electrodes based on thinner CNFs and higher mass loadings of MnO_2 NWs showed higher values of gravimetric and volumetric capacitances. This would be due to MnO_2 NWs forming a dense network in the thinner three-dimensional CNF framework. In addition, asymmetric supercapacitors with the MnO_2 NW/CNF composite electrode as the positive electrode and activated carbon as the negative electrode showed high energy and power densities of 8.9 W h kg^{-1} and 4.9 kW kg^{-1}, respectively. These results clearly indicate that the hierarchical network nanostructure composed of an active material and a charge collector can be considered a promising electrode for various electrochemical devices.

Introduction

To improve the capacity of electrochemical supercapacitors, a wide range of metal oxides such as ruthenium oxide (RuO_2),[1,2] manganese dioxide (MnO_2),[3] vanadium oxide (V_2O_5),[4] and nickel oxide (NiO)[5] have been investigated as the active electrode materials and show promising characteristics. Among them, MnO_2 with its high theoretical specific capacitance (1370 F g^{-1}), natural abundance and environmental friendliness, as well as low cost, has received considerable attention.[6] However, it is known that MnO_2 shows a high specific capacitance only at very low loadings (about a few μg cm^{-2}) on the current collector due to its extremely low electrical conductivity (10^{-5} to 10^{-6} S cm^{-1}).[3,6–8] Therefore, the development of high specific capacitance electrodes with MnO_2 is still a challenge. To overcome this issue, many approaches, such as doping of MnO_2,[9]

nanofabrication of MnO_2,[10] and composite formation using conductive materials[11,12] have been taken. In particular, formation of composite electrodes using nanostructured MnO_2 and conductive carbonaceous materials have attracted much attention.[13–16] For example, several researchers reported MnO_2 electrodes mixed with carbon microfibers,[17] carbon nanotubes (CNT),[18,19] graphene[20–22] and a CNT/graphene complex.[23,24]

Herein, we fabricated hierarchically nanostructured composite electrodes, MnO_2 nanowires (MnO_2 NWs) on carbon nanofiber (CNF) webs. The hierarchical nanostructure allows efficient charge collection through the three-dimensional (3-D) CNF framework (Fig. 1). Therefore, it is expected that this composite electrodes can simultaneously achieve high capacitance and rapid charge and discharge due to the high mass loading of the MnO_2 NWs on the conductive CNF webs with high surface area. In the present study, MnO_2 NW/CNF composite electrodes were prepared by the electrodeposition of MnO_2 NWs with various mass loadings on the electrospun CNFs with diameters of 250 and 650 nm. We investigated the effects of CNF diameters and mass loadings of MnO_2 NWs on the hierarchical nanostructure formation and the performance of the composite electrodes. In addition, we fabricated asymmetric supercapacitor (ASC) devices with the MnO_2 NW/CNF composite electrode as the positive electrode and activated carbon (AC) as the negative electrode and evaluated their performance.

[a] Department of Materials Science and Engineering, Tokyo Institute of Technology, 2-12-1 Ookayama, Meguro-ku, Tokyo 152-8552, Japan. E-mail: matsumoto.h.ac@m.titech.ac.jp

[b] Department of Chemical Science and Engineering, Tokyo Institute of Technology, 4259, Nagatsuta-cho, Midori-ku, Yokohama-shi 226-8502, Japan

[c] Department of Micro and Nanotechnology, Middle East Technical University, Ankara 06800, Turkey

[d] Department of Metallurgical and Materials Engineering, Middle East Technical University, 06800 Ankara, Turkey
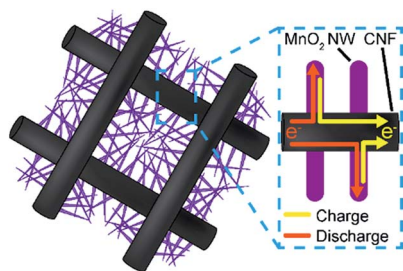
Fig. 1 Schematic of hierarchically nanostructured composite electrode, MnO_2 NWs on CNF web.

Experimental procedure

Materials

Polyacrylonitrile (PAN, M_w = 150 000) was purchased from Sigma-Aldrich, USA. *N,N*-Dimethylformamide (DMF) of extrapure grade and manganese(ii) acetate tetrahydrate ((CH_3-$COO)_2Mn \cdot 4H_2O$)) of extra-pure grade were obtained from Wako Pure Chemical Industries, Japan. Sodium sulfate of extrapure grade and hydrochloric acid of extrapure grade were obtained from Kanto Chemical, Japan. These reagents were used without further purification. Activated carbon sheet (AC sheet, the specific capacitance is 82.2 F g^{-1} at 1.0 A g^{-1}) was obtained from Nippon Valqua Industries, Japan.

Preparation of CNF webs

The CNF webs were prepared by electrospinning of a precursor polymer solution and successive stabilization and carbonization.[25–27] Polyacrylonitrile (PAN) was used as the carbon precursor.[28] For preparation of the spinning solution, PAN was dissolved in DMF to give 10 and 15 wt% PAN/DMF solutions. The electrospinning device was the same as that used in our previous study.[29] The polymer solution was contained in a syringe with a stainless steel nozzle (0.21 mm internal diameter). The nozzle was connected to a high-voltage regulated DC power supply (HJPQ-30P1, Matsusada Precision, Japan). A constant volume flow rate was maintained by a syringe-type infusion pump (MCIP-III, Minato Concept, Japan). An aluminum plate (10 × 10 cm^2) was used as the collector for the electrospun fibers. The distance between the nozzle tip and the collector were 10 and 15 cm for the 10 and 15 wt% solutions, respectively. The applied voltage was 8 kV, and the flow rate was 5 μL min^{-1}. All spinnings were carried out at 25 ± 3 °C and at a relative humidity value of less than 60%. The as-spun PAN nanofibers were heated at 230 °C for 3 h in air for stabilizing, then they were heated at 1000 °C for 1 h in a nitrogen atmosphere for carbonization.

Preparation of MnO_2 NW/CNF composite electrodes

The MnO_2 NW/CNF composite electrodes were prepared by electrodeposition of the MnO_2 NWs onto the CNF surfaces. Before the deposition, the CNF webs were sufficiently washed with acetone (Ac) and deionized water (DIW) to remove any contaminants. Subsequently, the CNF webs were soaked in a 0.1 M hydrochloric acid solution for 10 min for the surface modification with hydrophilic groups, washed thoroughly by DIW, then dried at 100 °C for 3 h under vacuum. Before electrodeposition, the CNF webs were cut into small pieces (1 cm × 2 cm) and the cut samples were immersed overnight in the mixed solution of Ac and DIW (Ac : DIW = 1 : 1 v/v) in order to promote infiltration of the electrodeposition solution. MnO_2 NWs were then deposited through the application of a constant voltage of 0.4 V (*vs.* Ag/AgCl sat.) in a solution containing 0.1 M ($CH_3COO)_2Mn \cdot 4H_2O$ and 0.1 M sodium sulfate (Na_2SO_4) at room temperature. The electrodepositions were carried out in a three-electrode cell with the CNF web as the working electrode, platinum mesh as the counter electrode, and a saturated Ag/AgCl electrode (DKK-TOA, Japan) as the reference electrode. The mass loading of the MnO_2 NWs was controlled by the charge passed at the range of 0.22, 0.55, 2.1 and 4.2 C cm^{-2}. After the deposition, the electrodes were removed from the electrodeposition solution and carefully washed with DIW to remove any excess electrolyte, then dried at 100 °C for 3 h under vacuum.

Characterization

The electrical conductivities along the surface direction of the CNF webs were measured by a four-point probe method using a low resistivity meter (Loresta-GP MCP-T610, Mitsubishi Chemical Analytech, Japan). The morphological characterization of the prepared composite electrodes were made by a field-emission scanning electron microscope (FE-SEM, S4700, Hitachi, Japan), a scanning electron microscope (SEM, JCM-5700, JEOL, Japan), and a transmission electron microscope (TEM, JEM-2010F, JEOL, Japan) operated at 100 kV. The pore size distribution of the MnO_2 NW/CNF composite electrodes was determined by mercury porosimetry measurements using an instrument (Auto Pore IV 9520, Micrometrics, USA). The crystal structure of the MnO_2 NWs was determined by an X-ray diffractometer (XRD, X'Pert-MPD, Philips, Netherlands). X-ray photoelectron spectroscopy (XPS) was conducted by an instrument (JPS-9010MC, JEOL, Japan) equipped with a monochromator using an Al anode (12 kV, 25 mA). The acquired spectra were charge-corrected using the Mn 2p(3/2) signal at 642.0 eV.

Electrochemical measurements

The electrochemical measurements of the MnO_2 NW/CNF composite electrodes were carried out using a potentiostat/galvanostat (SI 1287, Solartron ISA, UK), and a frequency response analyzer (1255B, Solartoron ISA, UK). The electrochemical characteristics of the prepared MnO_2 NW/CNF composite electrodes were determined by galvanostatic charge/discharge measurements in a three-electrode cell for plate-type electrodes (ALS, Japan). The composite electrode was used as the working electrode, platinum wire as the counter electrode, the Ag/AgCl electrode (3 M sodium chloride, NaCl) as the reference electrode, and a 1 M Na_2SO_4 solution as the electrolyte. Prior to the measurements, the composite electrode was soaked in the mixed solution of Ac and DIW (Ac : DIW = 1 : 1 v/v) for 1 h, then soaked overnight in a 1 M Na_2SO_4 solution.
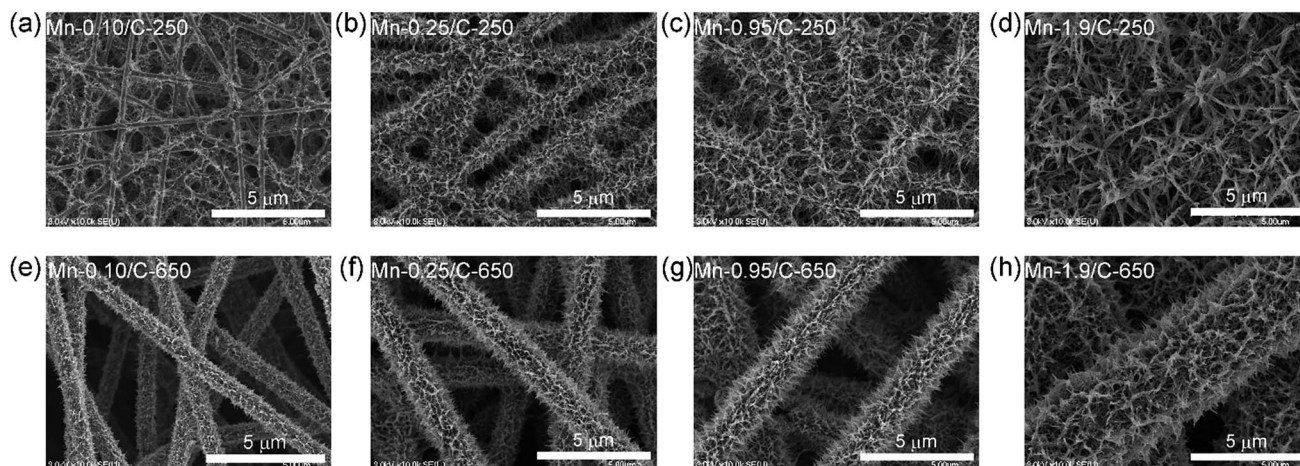
Fig. 2 Surface SEM images of MnO₂ NW/CNF composite electrodes with various mass loading: (a) Mn-0.10/C-250, (b) Mn-0.25/C-250, (c) Mn-0.95/C-250, (d) Mn-1.9/C-250, (e) Mn-0.10/C-650, (f) Mn-0.25/C-650, (g) Mn-0.95/C-650, and (h) Mn-1.9/C-650.

Fabrication and evaluation of the asymmetric supercapacitor devices

The ASC devices were fabricated using a two-electrode cell (Hosen, Japan) with the MnO₂ NW/CNF composite electrode as the positive electrode, an AC sheet as the negative electrode, Whatman cellulose filter as the separator between the two electrodes and a 1 M Na₂SO₄ solution as the electrolyte.

Results and discussion

Preparation and characterization of CNF webs and MnO₂ NW/CNF composite electrodes

The CNF webs with average diameters (D) of 256 ± 24 nm (C-250) and 667 ± 33 nm (C-650) were prepared by electrospinning from the 10 and 15 wt% PAN/DMF solutions, respectively, followed by successive carbonization (Fig. S1† shows SEM images of the prepared CNF webs and their diameter distribution). Thicknesses of the prepared webs were approximately 30 μm. C-250 and C-650 showed comparable apparent surface electric conductivities of 7.5 and 6.2 S cm^{-1}, respectively (Table S1†).[30]

MnO_2 NWs with the mass loading of 0.10, 0.25, 0.95, and 1.9 mg cm^{-2} were successfully deposited onto the CNF webs by changing the charge amounts based on eqn (1). Hereafter, the

Table 1 Structural characteristics of MnO₂ NW/CNF composite electrodes

Specific mass loading (mg cm^{-2})	Thickness of MnO₂ NW layer^a (μm)		MnO₂ content (wt%)	
	C-250	C-650	C-250	C-650
0.10	—	0.16 ± 0.06	46.5	20.8
0.25	0.17 ± 0.03	0.98 ± 0.15	59.3	59.1
0.95	—	1.26 ± 0.15	81.0	77.9
1.9	—	2.02 ± 0.24	84.7	86.3

^{a} The thickness of the MnO₂ NW layer was determined from SEM analysis on average of 50 points. The MnO₂ NW layer thickness of Mn/C-250s at 0.10, 0.95 and 1.9 mg cm^{-2} could not be determined, because MnO₂ NWs were partially deposited on the CNF surface at 0.10 mg cm^{-2} and MnO₂ NWs formed network structure in the interfiber space of the CNF framework.
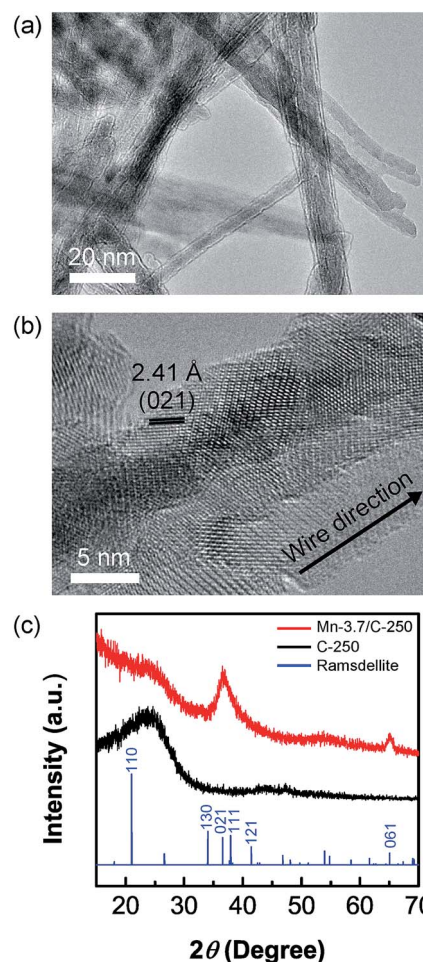

Fig. 3 (a) TEM image of MnO₂ NWs on Mn-0.95/C-250 electrode. (b) Higher magnification image of (a). (c) XRD patterns of Mn-3.7/C-250 electrode, C-250, and ramsdellite (ICDD: 042-1316).

prepared electrodes will be referred as Mn(-mass loading)/C-(-CNF diameter) (*e.g.*, Mn-0.10/C-250).
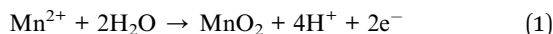
$$Mn^{2+} + 2H_2O \rightarrow MnO_2 + 4H^+ + 2e^- \tag{1}$$

Fig. 2 shows SEM images of the MnO_2 NW/CNF composite electrodes with various mass loadings. For the Mn/C-250s, MnO_2 NWs mainly grew on the intersection points of CNF framework at the small mass loading of 0.10 mg cm^{-2} (Fig. 2(a)). With an increase in the mass loading, MnO_2 NWs covered the surface of the CNFs and formed a layer structure (@0.25 mg cm^{-2}, Fig. 2(b)). Finally, MnO_2 NWs were densely grown and formed a network structure in the inter-fiber space of the CNF framework (@0.95 and 1.9 mg cm^{-2}, Fig. 2(c) and (d), respectively): hierarchical network nanostructures composed of an active material and a charge collector was formed. On the other hand, for the Mn/C-650s (Fig. 2(e–h)), MnO_2 NW did not form a network structure, but formed a thick layer on the surface of CNF at the higher mass loading (Table 1). The difference in the hierarchical structure between Mn/C-250s and Mn/C-650s is due to the differences in the surface area and the size of inter-fiber space between CNF frameworks.

The TEM images demonstrate that MnO_2 NWs grown on all the electrodes have high aspect ratios (several hundred nanometers in length and 5–20 nm in diameter). The MnO_2 NWs were composed of aggregations of needle-like fine crystals with individual diameters of 2–5 nm (Fig. 3(a) and (b)). To identify the crystal structure of the MnO_2 NWs, a large amount of MnO_2 NWs (3.7 mg cm^{-2}) were deposited onto C-250 electrode. The

Table 2 Specific capacitance of MnO_2 NW/CNF composite electrodes at a current density of 0.5 A g^{-1}

Specific mass loading (mg cm^{-2})	C_g (F g^{-1})		C_v (F cm^{-3})		C_g-MnO_2 (F g^{-1})	
	C-250	C-650	C-250	C-650	C-250	C-650
0.10	124	43.4	18.7	10.6	266	209
0.25	134	123	48.1	24.7	227	208
0.95	165	146	74.7	44.5	204	188
1.9	125	109	52.4	28.3	148	127

XRD patterns of the Mn-3.7/C-250 and C-250 are provided in Fig. 3(c). Peak positions of ramsdellite phase are provided in the same figure for comparison. There are two characteristic peaks around 37 and 65 degrees for Mn-3.7/C-250, which corresponds to the (021) and (061) planes of ramsdellite, but the other ramsdellite peaks are very weak and cannot be clearly observed. Chabre and some other researchers reported that the electrochemically-prepared MnO_2 preferentially grows perpendicular to the (021) and (061) planes with a large concentration of structural defects called microtwinning.[31–33] The chemical defects of microtwinning are known to be compensated by OH^-/O^{2-} in twinned boundaries.

XPS results also indicate the existence of a large amount of structural water in the MnO_2 NWs as discussed in ESI (Table S2 and Fig. S2†).[31] In addition, the continuous twinning of the crystal phase was clearly observed in the deposited MnO_2 NWs through high-magnification TEM analysis (Fig. 3(b)). This also supports the fact that the axis of MnO_2 NWs would correspond either to the direction (021) or (061), and MnO_2 NWs contain a number of twin boundaries.

Electrochemical measurements of MnO_2 NW/CNF composite electrodes

Fig. 4(a) and (b) show the charge–discharge curves of Mn/C-250s and Mn/C-650s with various mass loadings at a current density of 0.5 A g^{-1}, respectively. All the MnO_2 NW/CNF composite electrodes show triangular curves: the larger amount of MnO_2 NW-deposited electrode shows a smaller slope than unmodified CNF electrodes, demonstrating better capacitance.

The specific gravimetric capacitance for total electrode mass (C_g) and deposited MnO_2 NWs (C_g-MnO_2), and the specific volumetric capacitance for apparent volume of electrode (C_v)
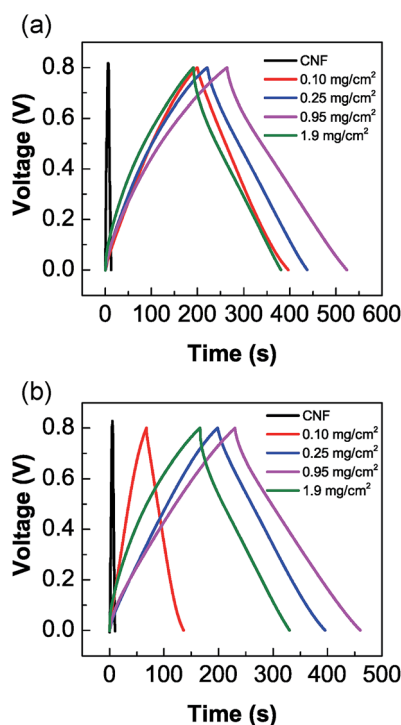

Fig. 4 Charge–discharge curves of (a) Mn/C-250 and (b) Mn/C-650 composite electrodes with various mass loadings at a current density of 0.5 A g^{-1}.

Table 3 The internal structural characteristics of Mn-0.95/C-250 and Mn-0.95/C-650 composite electrodes

Electrode	Average pore size^a (µm)	Porosity^a (%)
C-250	0.83	61
C-650	2.69	57
Mn-0.95/C-250	0.12	34
Mn-0.95/C-650	2.72	63

^{a} Determined by mercury porosimetry measurements in the pore size ranging from 3 nm to 10 µm.
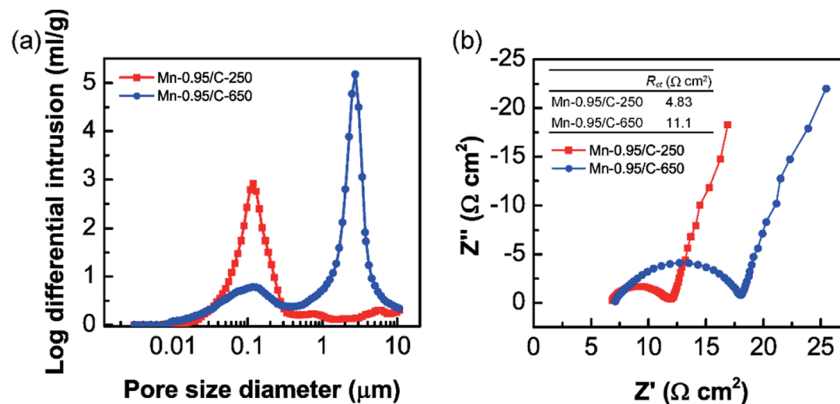
Fig. 5 (a) Pore size distributions of Mn-0.95/C-250 and Mn-0.95/C-650 electrodes in the range from 3.0 nm to 10 μm. (b) Nyquist plots of Mn-0.95/C-250 and Mn-0.95/C-650 electrodes.

(the definitions are included in the ESI†) were evaluated by galvanostatic charge/discharge measurements as shown in Table 2. The Mn-0.95/C-250 electrode showed the highest C_g of 165 F g^{-1}, which is better than the reported C_g of 120–150 F g^{-1} for the MnO$_2$/carbon composite electrodes including MnO$_2$ nanofiber/carbon nanosphere, MnO$_2$ nanoparticle/CNT, and MnO$_2$ nanoflower/graphene electrodes.[16,34,35] Mn/C-250s show higher gravimetric and volumetric capacitances than those of Mn/C-650s at all the mass loadings. In addition, Mn/C-250s and Mn/C-650s show the maximum value of C_g and C_v at the mass loading of 0.95 mg cm^{-2}. This can be explained by the assumption that the electrochemically utilizations of MnO$_2$ NWs were substantially decreased at the mass loading of 1.9 mg cm^{-2} due to its small electric conductivities. The assumption

was supported by a relatively large decrease in C_g-MnO$_2$ at the greater mass loading of MnO$_2$.

The difference in the capacitances between Mn/C-250s and Mn/C-650s more significantly appeared in volumetric capacitance than in gravimetric one. It would be due to the contribution of the internal structure of the MnO$_2$ NW/CNF composite electrodes. To further investigate the structure–capacitance relationship of the MnO$_2$ NW/CNF composite electrodes, the internal structural characteristics of the Mn-0.95/C-250 and the Mn-0.95/C-650 are summarized in Table 3 (pore size distribution is also shown in Fig. 5(a)). For the Mn-0.95/C-250, only a large number of nanosized pores, which correspond to the interspace between the MnO$_2$ NWs, appeared. For the Mn-0.95/C-650, on the other hand, both a small number of nanosized pores and a large number of microsized pores, which correspond to the
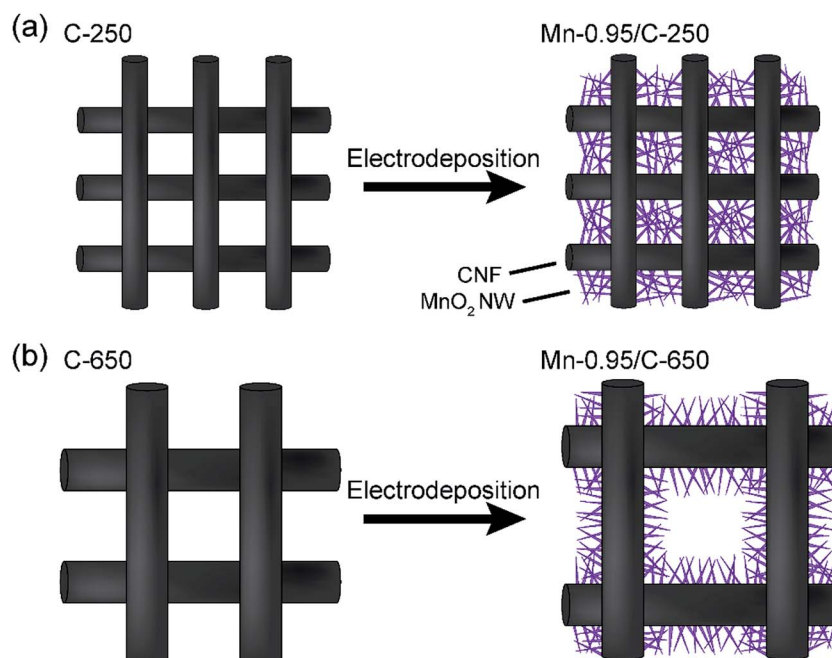

Fig. 6 (a and b) Schematics of the internal structures of the CNF electrodes before and after electrochemical deposition of MnO$_2$ NWs for C-250 and C-650, respectively.

interspaces between the MnO_2 NWs and surface-modified CNFs, respectively, appeared. As shown in Table 3, after electrodeposition of MnO_2 NWs, the pore size of the C-250 decreased from 0.83 μm to 0.12 μm while that of C-650 was slightly increased from 2.69 μm to 2.72 μm. In addition, the porosity of the C-250 significantly decreased by the electrodeposition of MnO_2 NWs, but that of C-650 was slightly increased from 57% to 63% as well as pore size (the MnO_2 NW layer deposited on C-650 framework enlarge the inter-fiber space. This behaviour was also confirmed by the thickness change of the electrodes, see Fig. S3†). These internal structural changes are due to the difference in the hierarchical nanostructure between Mn/C-250 and Mn/C-650 composite electrodes: for the Mn-0.95/C-250, the MnO_2 NWs form a network nanostructure in the CNF framework because of its narrow inter-fiber space.

Based on these structural characteristics, the findings that Mn-0.95/C-250 showed higher capacitance than Mn-0.95/C-650 could be explained by the following assumptions. At the high mass loading of Mn/C-250, formation of more densely network structure of MnO_2 NWs in the CNF framework would enhance electrochemically utilization efficiency of MnO_2 (Fig. 6(a)). On the contrary, at the high mass loading of Mn/C-650, the thick MnO_2 NW layer with small electric conductivities[6,32] would reduce electrochemically utilization efficiency of MnO_2 (Fig. 6(b)). This is also supported by electrochemical impedance measurements: the charge transfer resistances (R_{ct}) of the Mn-0.95/C-250 is lower than half of that of the Mn-0.95/C-650 (Fig. 5(b)).

Fabrication and evaluation of the asymmetric supercapacitor

To confirm an applicability of the MnO_2 NW/CNF composite electrodes for the supercapacitor electrode, an ASC device was fabricated and the device performance was evaluated. The device configuration is schematically shown in Fig. 7(a). Mn-0.95/C-250 electrode, AC, and 1 M Na_2SO_4 solution were used as the positive electrode, the negative electrode and the electrolyte, respectively. As shown in Fig. 7(b), the ASC operated at a voltage window of 1.6 V and achieved a capacitance of 25.1 F g^{-1} at a current density of 1.0 A g^{-1}. This result compares with the previous works: MnO_2 nanopowder and AC electrodes (22 F g^{-1} at 1.1 A g^{-1}), MnO_2 nanofiber/carbon nanosphere and carbon nanosphere electrodes (24.5 F g^{-1} at 1.0 A g^{-1}), and MnO_2 nanopowder and graphene electrodes (about 27 F g^{-1} at 1.0 A g^{-1}).[16,36,37] The energy and power densities (the definitions are included in the ESI†) of the ASC showed high values of 8.9 W h kg^{-1} and 4.9 kW kg^{-1} at 1.0 A g^{-1}, respectively. For comparison with other ASCs prepared with MnO_2 and carbonaceous materials, the Ragone plot is shown in Fig. 7(c).[10,16,37–40] Fig. 7(d) shows the cyclic performance and coulombic efficiency of the ASC at a current density of 1.0 A g^{-1}. This device showed a capacitance retention of 80% and high coulombic efficiency (>99%) after 2000 cycles. The decrease in capacitance would derive from the morphological change in the MnO_2 NWs on the positive electrode because the AC negative electrode have good cycle stability (>97% after 2000 cycles). Fig. S4† shows the SEM image of Mn-0.95/C-250 electrode after 2000 cycles. The as-
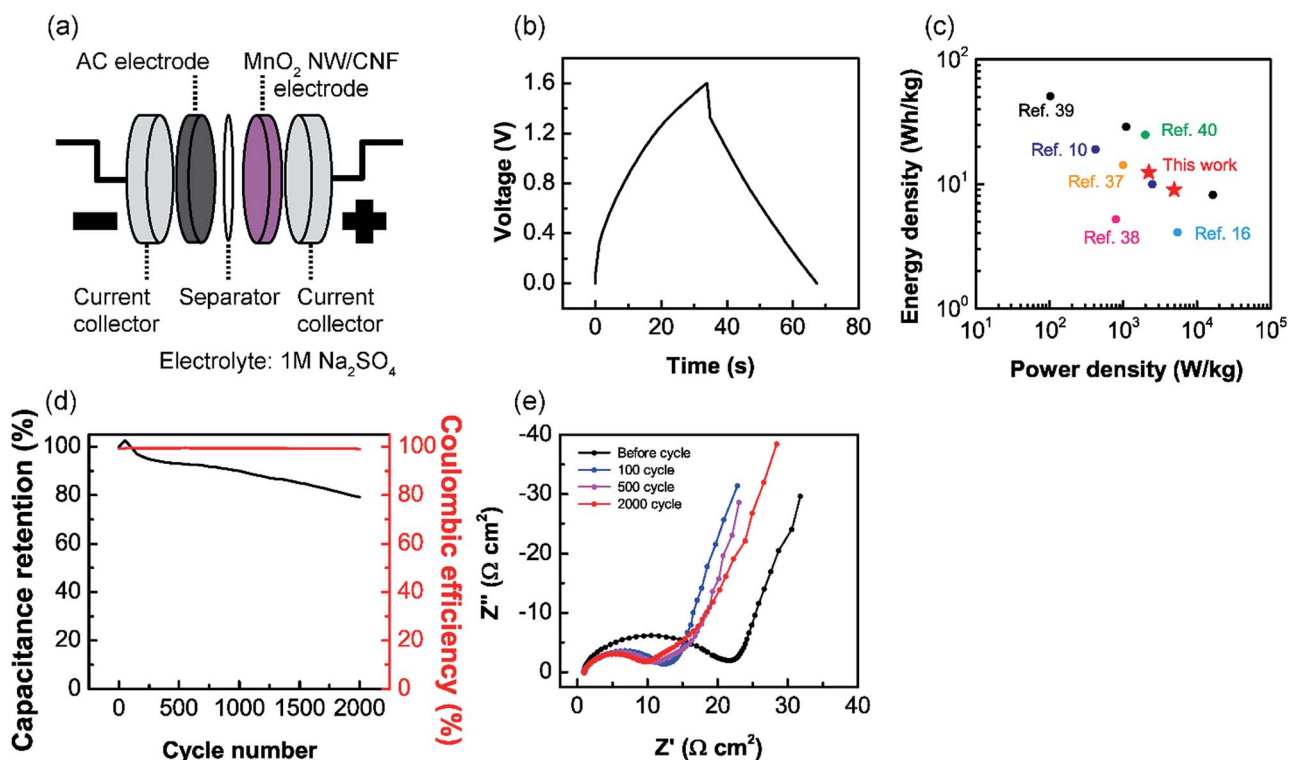

Fig. 7 (a) Schematic configuration of the ASC device. (b) Galvanostatic charge/discharge curves of the ASC measured at a current density of 1.0 A g^{-1}. (c) Ragone plot of energy density *versus* power density for the fabricated ASC and other ASCs with MnO_2 and carbonaceous composite electrode materials reported in literatures. (d) Cyclic performance and coulombic efficiency of the ASC at a current density of 1.0 A g^{-1}. (e) Nyquist plots of the ASC during cycling test at a current density of 1.0 A g^{-1}.

prepared MnO_2 NWs were converted into a film-like structure at the electrolyte interface. Nyquist plots of the ASC during cycling test at a current density of 1.0 A g^{-1} are shown in Fig. 7(e). After 500 cycles, a new constant inclination (45° angle) region clearly appears in low-frequency range. The appearance of this region indicates the increase in diffusion length of ions and support the morphological change in the MnO_2 NWs.[41,42] This morphological change would be caused by slow dissolution and re-deposition of MnO_2 during the electrochemical oxidation/reduction cycles and lead to a decrease in both the effective surface area and electric conductivities of the MnO_2. For the practical use of the MnO_2 NW/CNF composite electrodes, it will be a crucial issue to prevent the morphological change during the electrochemical oxidation/reduction cycles. Pang pointed out that the structural water in MnO_2 decrease the cycle stability.[3] As mentioned above MnO_2 NWs contain a large number of structural water. A thermal treatment is a possible approach to improve the cycling stability.

Conclusions

In the present study, hierarchically nanostructured composite electrodes were prepared by the electrodeposition of MnO_2 NWs on the electrospun CNF webs and the structure–property relationship of the MnO_2 NW/CNF composite electrodes was investigated. The internal structure of the composite electrodes depended on CNF diameter (or inter-fiber space of CNF framework) and loading amount of MnO_2 NWs: at a large mass loading of MnO_2, the deposited MnO_2 NWs form a network nanostructure between the interconnected C-250 framework, while a thicker MnO_2 NW layer was formed on the CNF surface in the C-650 framework. The electrodes based on the hierarchical structure composed of CNF framework and MnO_2 NW network showed high gravimetric and volumetric capacitances. An asymmetric supercapacitor shows high energy and power densities of 8.9 W h kg^{-1} and 4.9 kW kg^{-1}, respectively, and 80% capacitance retention and high coulombic efficiency (>99%) over 2000 cycles. This result clearly suggests hierarchical network nanostructure composed of an active material and a charge collector enhance the electrochemically utilization efficiency of MnO_2 on the electrode surface. These findings provide a useful guide in design of efficient electrochemical device electrodes including supercapacitors.

Acknowledgements

References

1 D. Galizzioli, F. Tantardini and S. Trasatti, *J. Appl. Electrochem.*, 1974, **4**, 57–67.

2 S. Trasatti and G. Buzzanca, *J. Electroanal. Chem. Interfacial Electrochem.*, 1971, **29**, A1–A5.

3 S. Pang, M. A. Anderson and T. W. Chapman, *J. Electrochem. Soc.*, 2000, **147**, 444–450.

4 H. Y. Lee and J. B. Goodenough, *J. Solid State Chem.*, 1999, **148**, 81–84.

5 V. Srinivasan and J. W. Weidner, *J. Electrochem. Soc.*, 1997, **144**, L210–L213.

6 M. Toupin, T. Brousse and D. Bélanger, *Chem. Mater.*, 2004, **16**, 3184–3190.

7 J. N. Broughton and M. J. Brett, *Electrochim. Acta*, 2005, **50**, 4814–4819.

8 C. Xu, F. Kang, B. Li and H. Du, *J. Mater. Res.*, 2010, **25**, 1421–1432.

9 J. Kang, A. Hirata, L. Kang, X. Zhang, Y. Hou, L. Chen, C. Li, T. Fujita, K. Akagi and M. Chen, *Angew. Chem., Int. Ed.*, 2013, **52**, 1664–1667.

10 M. Huang, Y. Zhang, F. Li, L. Zhang, R. S. Ruoff, Z. Wen and Q. Liu, *Sci. Rep.*, 2014, **4**, 3878.

11 Q. Tang, M. Chen, C. Yang, W. Wang, H. Bao and G. Wang, *ACS Appl. Mater. Interfaces*, 2015, **7**, 15303–15313.

12 T. G. Yun, B. il Hwang, D. Kim, S. Hyun and S. M. Han, *ACS Appl. Mater. Interfaces*, 2015, **7**, 9228–9234.

13 T. Zhai, F. Wang, M. Yu, S. Xie, C. Liang, C. Li, F. Xiao, R. Tang, Q. Wu, X. Lu and Y. Tong, *Nanoscale*, 2013, **5**, 6790–6796.

14 G. Yu, L. Hu, M. Vosgueritchian, H. Wang, X. Xie, J. R. McDonough, X. Cui, Y. Cui and Z. Bao, *Nano Lett.*, 2011, **11**, 2905–2911.

15 J. Liu, J. Essner and J. Li, *Chem. Mater.*, 2010, **22**, 5022–5030.

16 Z. Lei, J. Zhang and X. S. Zhao, *J. Mater. Chem.*, 2012, **22**, 153–160.

17 M.-S. Wu, Z.-S. Guo and J.-J. Jow, *J. Phys. Chem. C*, 2010, **114**, 21861–21867.

18 L. Hu, W. Chen, X. Xie, N. Liu, Y. Yang, H. Wu, Y. Yao, M. Pasta, H. N. Alshareef and Y. Cui, *ACS Nano*, 2011, **5**, 8904–8913.

19 P. Li, Y. Yang, E. Shi, Q. Shen, Y. Shang, S. Wu, J. Wei, K. Wang, H. Zhu, Q. Yuan, A. Cao and D. Wu, *ACS Appl. Mater. Interfaces*, 2014, **6**, 5228–5234.

20 M. Yang, K. G. Lee, S. J. Lee, S. B. Lee, Y.-K. Han and B. G. Choi, *ACS Appl. Mater. Interfaces*, 2015, **7**, 22364–22371.

21 J. Deng, X. Wang, X. Duan and P. Liu, *ACS Sustainable Chem. Eng.*, 2015, **3**, 1330–1338.

22 B. Shen, J. Lang, R. Guo, X. Zhang and X. Yan, *ACS Appl. Mater. Interfaces*, 2015, **7**, 25378–25389.

23 Y. Cheng, S. Lu, H. Zhang, C. V. Varanasi and J. Liu, *Nano Lett.*, 2012, **12**, 4206–4211.

24 Y. Jin, H. Chen, M. Chen, N. Liu and Q. Li, *ACS Appl. Mater. Interfaces*, 2013, **5**, 3408–3416.

25 A. Greiner and J. H. Wendorff, *Angew. Chem., Int. Ed.*, 2007, **46**, 5670–5703.

26 D. Li and Y. Xia, *Adv. Mater.*, 2004, **16**, 1151–1170.

27 D. H. Reneker and A. L. Yarin, *Polymer*, 2008, **49**, 2387–2425.

28 A. Krueger, *Carbon Materials and Nanotechnology*, Wiley-VCH Verlag GmbH & Co. KGaA, Weinheim, Germany, 2010.

29 H. Matsumoto, S. Imaizumi, Y. Konosu, M. Ashizawa, M. Minagawa, A. Tanioka, W. Lu and J. M. Tour, *ACS Appl. Mater. Interfaces*, 2013, **5**, 6225–6231.

30 S. Imaizumi, H. Matsumoto, K. Suzuki, M. Minagawa, M. Kimura and A. Tanioka, *Polym. J.*, 2009, **41**, 1124–1128.

31 Y. Chabre and J. Pannetier, *Prog. Solid State Chem.*, 1995, **23**, 1–130.

32 P. Ruetschi, *J. Electrochem. Soc.*, 1984, **131**, 2737–2744.

33 P. Ruetschi and R. Giovanoli, *J. Electrochem. Soc.*, 1988, **135**, 2663–2669.

34 M. Narubayashi, Z. Chen, K. Hasegawa and S. Noda, *RSC Adv.*, 2016, **6**, 41496–41505.

35 Y. He, W. Chen, X. Li, Z. Zhang, J. Fu, C. Zhao and E. Xie, *ACS Nano*, 2013, 174–182.

36 T. Brousse, M. Toupin and D. Bélanger, *J. Electrochem. Soc.*, 2004, **151**, A614–A622.

37 A. Mery, F. Ghamouss, C. Autret, D. Farhat and F. Tran-Van, *J. Power Sources*, 2016, **305**, 37–45.

38 Y. S. Wang, D. S. Tsai, W. H. Chung, Y. S. Syu and Y. S. Huang, *Electrochim. Acta*, 2012, **68**, 95–102.

39 Z. Fan, J. Yan, T. Wei, L. Zhi, G. Ning, T. Li and F. Wei, *Adv. Funct. Mater.*, 2011, **21**, 2366–2375.

40 P. Shang, J. Zhang, W. Tang, Q. Xu and S. Guo, *Adv. Funct. Mater.*, 2016, **26**, 7766–7774.

41 W. Sugimoto, H. Iwata, K. Yokoshima, Y. Murakami and Y. Takasu, *J. Phys. Chem. B*, 2005, **109**, 7330–7338.

42 S.-E. Chun, S.-I. Pyun and G.-J. Lee, *Electrochim. Acta*, 2006, **51**, 6479–6486.